Advances in Science and Technology Research Journal

Advances in Science and Technology Research Journal, 2025, 19(5), 31–45
https://doi.org/10.12913/22998624/201250
ISSN 2299-8624, License CC-BY 4.0

Received: 2025.01.06
Accepted: 2025.03.14
Published: 2025.04.01

Dynamics modeling and analysis of six-bar planar linkage mechanism with flexible coupler-links

Sy Nam Nguyen[1], Duc Hieu Tran*[1]

[1] Hanoi University of Civil Engineering, Hanoi, Vietnam
* Corresponding author's e-mail: hieutd@huce.edu.vn

ABSTRACT

Advanced materials are widely used in machine mechanisms, along with the requirement that the mechanical structure of the mechanism must be compact and slim to reduce inertia, save energy and increase working speed. However, this leads to elastic deformation affecting movement, accuracy and causing delays in sequential operations. In this paper, a six-bar linkage planar mechanism is combined from two four-bar linkage mechanisms. In which the connecting rods are considered as general elastic elements that are both compressive and bending. By representing the elastic rods by the modal synthesis technology, combined with the use of multi-body dynamics methods, which are the multiplier Lagrange equations, the paper has established a nonlinear differential-algebraic system of motion. From this system of equations, the study has numerically investigated some cases of forward dynamics to make assessments and comments on the influence of elastic deformation on the motion, the accuracy of the working position of the mechanism, and the significance of numerical investigation in the design of mechanical structures. This dynamic model can be used for other problems such as periodic oscillation of elastic mechanisms, linearization and investigation of motion stability, or control of motion and elastic oscillation.

Keywords: constrained multibody systems, differential–algebraic equations, flexible mechanism, six-bar mechanism, Watt II.

INTRODUCTION

Modern machine designs often aim for compact, slender structures and the use of advanced materials to increase working speed, save energy, and reduce inertia. However, this leads to significant deformation of components, especially long, slender components or those moving at high speeds. Such deformation causes vibrations during operation, significantly increasing the reaction forces at joints. These vibrations also reduce precision in mechanisms requiring high accuracy and delay sequential operations due to the persistence of vibrations over a certain period. This necessitates more accurate dynamic research methods that reflect the material properties and account for the effects of the deformation components of the mechanism.

Studies on flexible multibody dynamics have been conducted early [1-5]. To study this issue, scientists often start by constructing mathematical models from mechanical models. To construct mathematical models, studies mainly use three methods [1]: the floating frame of reference formulation, linear theory of elastodynamics and finite segment method. The first method is the most commonly used. In this method, the large displacements of the system and the deformations of elastic materials are determined using two sets of coordinates. The first set includes coordinates that define the position and orientation of the relative coordinate system attached to each elastic material. The second set consists of elastic coordinates

that determine the relative deformation of the elastic material within the coordinate system attached to the material. The elastic coordinates can be represented using methods such as the component mode method, the finite element method, or experimental identification techniques.

In systems with multiple elastic components, flexible robot manipulators have been studied the most extensively and comprehensively [1, 6, 7]. Research on elastic mechanisms, however, has primarily focused on simple mechanisms such as four-bar linkages [8-12], cam mechanisms [13-14], slider-crank mechanisms [15-16], culit mechanisms, or three-link mechanisms with internal driving links [17]. Sung and Chen [18] proposed an optimal control method to suppress vibrations in a four-bar hinged mechanism where the driven link (the actuated link) is an elastic member. They utilized piezoceramic sensors and an actuator mounted on the elastic link for control. However, the influence of elastic deformation and the control of the mechanism's motion were not considered, as the authors used a model with only a single joint. Beale and Lee [15] studied the feasibility of applying fuzzy control to a slider crank mechanism, a piezoelectric induction motor was placed on the elastic link to realize the control requirements. Liao et al. [16] also proposed the use of piezoelectric membranes and designed a robust controller based on the linear state space model of the mechanism. The effects of parametric oscillations and instabilities caused by the control operation were studied. In the study of Karkoub and Yigit [9], the authors performed vibration control of a four-link mechanism with an elastic connecting rod subjected to bending only (ignoring axial deformation) by applying a moment to the connecting link to limit the influence of elastic deformation. The authors used a PD controller, to verify the effectiveness of the controller, the authors simulated the control of the mechanism at the equilibrium position when giving the connecting rod an initial bending deformation, resulting in the deformation being eliminated, the mechanism remained in equilibrium. With the control of vibration through the guide, the control becomes much simpler. Khang et al. [10] studied the dynamics of a four-bar mechanism in which the connecting rod is subjected to both transverse bending and axial tension-compression. They controlled the vibrations of the mechanism via the driving link using a PD controller. In studies [20-23], the authors sought simpler solutions to such problems by linearizing the nonlinear equations of motion.

Studies on complex elastic mechanisms that are coupled from the above simple mechanisms have not received much attention due to the complexity of elastic elements and the large amount of calculations, so they mainly focus on studying the dynamics and control problems of rigid mechanisms. The article [24] studies and analyzes the kinematics of a six-bar linkage mechanism, the kinematic relationship between the input-output link and the actuator-output link is studied, in this study the links are solid objects. In the study [25], the machine mechanism is a combination of a four-link mechanism and a cam mechanism, in which the joint clearances and the elasticity of the connecting rod are considered. The authors use the Kean equation to establish a mathematical model, in which the finite element method is used in combination with the method of analysis in a specific form. Next, numerical surveys are carried out to make comments and evaluate the influence of clearances, elasticity and materials on the working accuracy when the mechanism moves quickly. The study [26] considers the influence of lubrication clearances and deformable components on the operation of a multi-link mechanism with the dynamic equation established by Lagrange multiplier method. In the study [27], the jumping ability of organisms was modeled as a one-degree-of-freedom Watt-type six-bar mechanism. Each jumping leg consisted of multiple flexible links and a flexible joint, leading to the establishment of a rigid-flexible dynamic model. Based on this model, the impact of structural and installation parameters on jumping performance was analyzed. In [28], the authors utilized a complex mechanism consisting of a basic four-bar linkage combined with an additional structural group (resembling a slider-crank mechanism) to create dwell linkage mechanisms. However, this study did not investigate the deformation of the links.

The six-bar linkages mechanism are typical mechanisms in machinery, formed by two four-bar mechanisms. It performs the function of converting the rotary motion of the input shaft into the oscillating motion of the output shaft, with variable speed. Depending on the speed and the oscillation stroke of the output link, the geometric dimensions and the arrangement of the mechanism's links are designed. Such mechanisms, when combined with cam mechanisms,

planetary gear systems, belt drives, and pulley systems, form various systems [24] for purposes such as: connecting air conditioning compressors to the main engine of automobiles, controlling valve motion in engines, powering lawn mowers or tractors, and improving the wheel drive systems of gardening equipment. In document [33], a six-bar mechanism is designed with a primary application that includes gripping empty bottles lying flat on an input conveyor, rotating, aligning, and placing them upright on another conveyor. In [34], six-bar linkages are the next basic single degree-of-freedom closed kinematic chains after the four-bar linkage that are examined. They are classified into two main configurations: Watt chains and Stephenson chains. These two configurations give rise to five distinct types of six-bar linkages, referred to as Watt I, Watt II, Stephenson I, Stephenson II, and Stephenson III. This study focuses on the kinematic synthesis of rigid six-bar linkages for function, motion, and path generation. These six-bar linkages were chosen due to their enhanced design flexibility compared to four-bar linkages.

Based on the study of reference documents, it is shown that the study of complex elastic mechanisms is very necessary to be studied, so this study builds a dynamic model for a six-bar linkage mechanism with Watt II type that is coupled from two four-bar linkage mechanisms, in which the elastic components are connecting rods. The study uses the floating frame of reference formulation method, the elastic components are represented by the method (modal synthesis technology/component modes), from which the Lagrange multiplier method/ Lagrange's equation with multiplier is used to establish the dynamic model. From this dynamic model, the study will conduct some numerical surveys to evaluate the influence of the elastic factor on the motion and working accuracy of the six-bar linkage mechanism.

MECHANICAL AND DYNAMICS MODEL

Mechanical model

The planar six-bar linkage mechanism with Watt II type is composed of two four-bar linkage mechanisms, one form of which has the diagram shown in Figure 1, where O_1ABO_2 is the first four-linkage mechanism, O_2CDO_3 is the second four-linkage mechanism. In this mechanism, O_1A is the input crank (or input link), O_3D is the output link, link AB and link CD are connecting rods.

In this mechanism, the long-links and slender-links have a significant influence on the motion due to their deformation, so they are considered as flexible-bodies, such as the connecting rods (AB and CD). For links that are thick, short

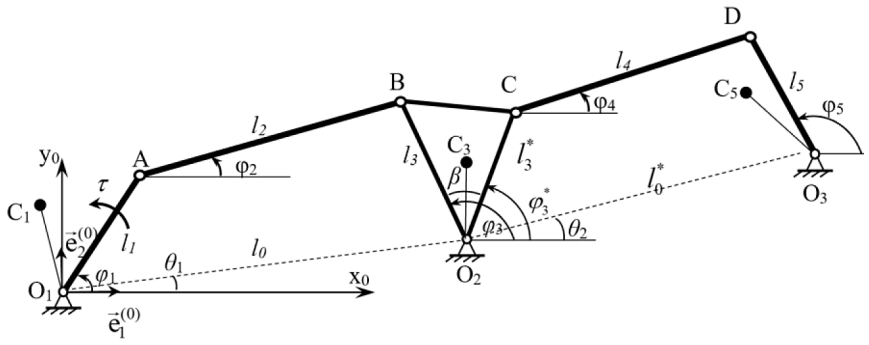

Fig. 1. Diagram of six-bar linkage planar mechanism

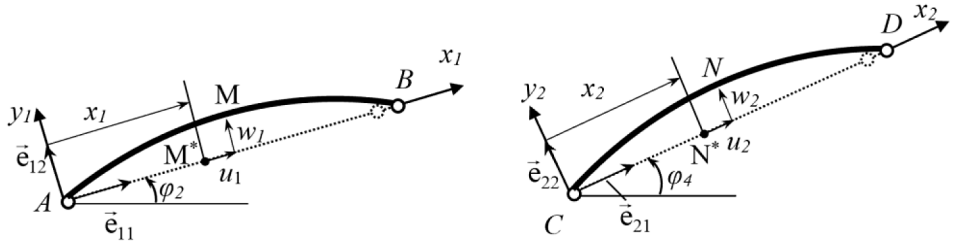

Fig. 2. Diagram floating frame of reference co-ordinates

and rigid, their deformation affects the movement of the mechanism insignificantly, so those links will be considered as rigid-links, such as the input-link O_1A, the swing link O_2BC and the output-link O_3D. Thus, O_1A-link is rigid-body with mass m_1, center of mass C_1, $O_1C_1 = s_1$, angle $AO_1C_1 = \alpha_1$, subjected to driving torque τ. AB-link is flexible link with mass m_2. O_2BC-link is rigid link with mass m_3, center of mass C_3, $O_2C_3 = s_3$, angle $BO_2C_3 = \alpha_3$, angle $BO_2C = \beta$. CD-link is flexible link with mass m_4. O_3D-link rigid link with mass m_5, center of mass C_5, $O_3C_5 = s_5$, angle $DO_3C_5 = \alpha_5$. The length of the links is $O_1A = l_1$, $AB = l_2$, $BO_2 = l_3$, $O_2C = l_3^*$, $CD = l_4$, $O_3D = l_5$, $O_1O_2 = l_0$, $O_2O_3 = l_0^*$.

Assume that: AB and CD are straight, homogeneous bars with constant cross-section, the axis of the bar coincides with the neutral axis when not deformed, the mechanism moves in the horizontal plane.

Dynamic model

To establish the dynamic model we use the floating frame reference method [1]. For elastic multibody systems with small elastic deformations, this method has many advantages such as: high accuracy, can use methods of multibody dynamics to establish dynamic equations of mechanicsm, dynamic equations written for rigid mechanicsm can be derived from equations written for elastic mechanicsm when the deformations are zero, etc. According to this method, the generalized coordinates that determine the movement of the links are the residual generalized coordinates because of the constrained multibody system. With the fix-coordinate system $O_1x_0y_0$, the angles φ_1, φ_2, φ_3, φ_4, φ_5 are the angles that determine the positions of the links as shown in Figure 1.

Elastic links are continuous systems characterized by an infinite number of degrees of freedom. Therefore, these links are often discretized into a system of finite degrees of freedom. There are many discretization methods, in this study we will discretize the elastic term using the commonly used method, the Ritz – Galerkin method (one of the assumed modes method). In this method the deformation of the elastic link is usually represented by a finite sum of the products of the spatial-eigenfunctions and the amplitude-time components.

$$w(x,t) = \sum_{i=1}^{N} X_i(x) q_i(t)\,;\; u(x,t) = \sum_{i=1}^{N} Y_i(x) p_i(t) \qquad (1)$$

where: $X_i(x)$ and $Y_i(x)$ are eigenfunctions (eigmodes) that satisfy the boundary conditions of the elastic connecting rods, and they are functions that can be determined based on these boundary conditions; $q_i(t)$, $p_i(t)$ are modal coordinates-time dependent; *i*–order is the order of the expansions.

To establish the dynamic equations of the constrained multibody system, we use the Lagrange's equation with multiplier combined with the constraint equations to form a system of differential-algebraic equations of motion. The equations of holonomic constrained multibody system with *n* generalized coordinates s_1, s_2, …, s_n (residual generalized coordinates system) has the form [29]:

$$\frac{d}{dt}\left(\frac{\partial T}{\partial \dot{s}_k}\right) - \frac{\partial T}{\partial s_k} = Q_k^* - \sum_{i=1}^{r} \lambda_i \frac{\partial f_i}{\partial s_k} \quad (k = 1,2,...,n) \qquad (2)$$

$$f_i(s_1, s_2, ..., s_n, t) = 0 \quad (i = 1,2,...,r) \qquad (3)$$

where: T is the kinematic energy of the system, Q_k^* is the generalized force corresponding to the generalized coordinates s_k

$$Q_k^* = -\frac{\partial \Pi}{\partial s_k} + Q_k\,,$$

with Π being the potential energy of the system, Q_k is the generalized force of non-conservative forces, f_i is the *i*th constraint equation, r is the total number of constraint equations, λ_i is the *i*th Lagrange multiplier. Thus, we have $(n+r)$ differential-algebraic equations to determine n generalized coordinates and r Lagrange multipliers λ_i.

Reference coordinate system Ax_1y_1 is attached to link AB with $Ax_1 \equiv$ AB (Fig.2a), Reference coordinate system Cx_2y_2 is attached to link CD with $Cx_2 \equiv$ CD (Fig.2b). Consider point *M* on link AB and point N on link CD with coordinates in the fixed coordinate system $O_1x_0y_0$ as (x_M, y_M) and (x_N, y_N), respectively. In the reference coordinate systems, the point M has coordinates $(x_1 + u_1, w_1)$ and point N has coordinates $(x_2 + u_2, w_2)$. Points A and C have coordinates (x_A, y_A) and (x_C, y_C) respectively in the fixed coordinate system. We have the formula to determine the coordinates of points M and N:

$$x_M = l_1\cos\varphi_1 + (x_1+u_1)\cos\varphi_2 - w_1\sin\varphi_2$$
$$y_M = l_1\sin\varphi_1 + (x_1+u_1)\sin\varphi_2 + w_1\cos\varphi_2$$
$$x_N = l_0\cos\theta_1 + l_3^*\cos\varphi_3^* + (x_2+u_2)\cos\varphi_4 - w_2\sin\varphi_4$$
$$y_N = l_0\sin\theta_1 + l_3^*\sin\varphi_3^* + (x_2+u_2)\sin\varphi_4 + w_2\cos\varphi_4$$

The boundary conditions of the flex-links AB and CD:

+ The transverse deformations at the two ends of the flex-links (in relative coordinate system) are:

$$w_1(0,t) = w_1(l_2,t) = 0,\ w_2(0,t) = w_2(l_4,t) = 0 \quad (4)$$

+ The longitudinal deformations at the two ends of the flex-links are:

$$u_1(0,t) = 0, u_1(l_2,t) = u_{1B}; u_2(0,t) = 0,\ u_2(l_4,t) = u_{2D} \quad (5)$$

The constraint equations:

$$f_1 = l_1cos\varphi_1 + (l_2 + u_{1B})cos\varphi_2 - l_3cos\varphi_3 - l_0cos\theta_1 = 0 \quad (6)$$
$$f_2 = l_1sin\varphi_1 + (l_2 + u_{1B})sin\varphi_2 - l_3sin\varphi_3 - l_0sin\theta_1 = 0 \quad (7)$$
$$f_3 = cos(\varphi_3 - \beta) + (l_4 + u_{2D})cos\varphi_4 - l_5cos\varphi_5 - cos\theta_2 = 0 \quad (8)$$
$$f_4 = sin(\varphi_3 - \beta) + (l_4 + u_{2D})sin\varphi_4 - l_5sin\varphi_5 - sin\theta_2 = 0 \quad (9)$$

with $\varphi_3^* = \varphi_3 - \beta$

The kinematic energy of the system:

$$T = \frac{1}{2}I_{O_1}\dot{\varphi}_1^2 + \frac{1}{2}I_{O_2}\dot{\varphi}_3^2 + \frac{1}{2}I_{O_3}\dot{\varphi}_5^2 + \frac{1}{2}\int_0^{l_2}\mu_1 v_M^2 dx_1 + \frac{1}{2}\int_0^{l_4}\mu_2 v_N^2 dx_2 \quad (10)$$

where: I_{O_1}, I_{O_2}, I_{O_3} are the inertia moments of links O_1A, BO_2C, DO_3 respectively; μ_1 and μ_2 (kg/m) are mass density of link AB and link CD respectively.

Strain potential energy of flex-links:

Using the Euler – Bernoulli beam theory for elastic links we have the strain potential energy:

$$\Pi = \frac{1}{2}E_1A_1\int_0^{l_2}\left(\frac{\partial u_1}{\partial x_1}\right)^2 dx_1 + \frac{1}{2}E_1I_1\int_0^{l_2}\left(\frac{\partial^2 w_1}{\partial x_1^2}\right)^2 dx_1 + \frac{1}{2}E_2A_2\int_0^{l_4}\left(\frac{\partial u_2}{\partial x_2}\right)^2 dx_2 + \frac{1}{2}E_2I_2\int_0^{l_4}\left(\frac{\partial^2 w_2}{\partial x_2^2}\right)^2 dx_2 \quad (11)$$

where E_1, A_1, I_1 and E_1, A_1, I_1 are respectively the elastic modulus, cross-sectional area, cross-sectional moment of inertia of rod AB and rod CD.

Assuming the deformation is small, transverse displacements do not affect longitudinal displacements and vice versa. Using the AMM, the transverse displacement and longitudinal displacement of the bars:

AB: $w_1(x_1,t) = \sum_{i=1}^{N_1} X_i^{(1)}(x_1)q_i^{(1)}(t)$, $u_1(x_1,t) = \sum_{k=1}^{N_2} Y_k^{(1)}(x_1)p_k^{(1)}(t)$ (12)

CD: $w_2(x_2,t) = \sum_{i=1}^{N_3} X_i^{(2)}(x_2)q_i^{(2)}(t)$, $u_2(x_2,t) = \sum_{k=1}^{N_4} Y_k^{(2)}(x_2)p_k^{(2)}(t)$ (13)

Using boundary conditions (4) and (5) we can derive the eigenfunctions:

$$X_i^{(1)} = \sin\left(\frac{i\pi}{l_2}x_1\right); \qquad X_i^{(2)} = \sin\left(\frac{i\pi}{l_4}x_2\right) \quad (14)$$

$$Y_k^{(1)}(x) = \sin\left(\frac{2k-1}{2}\frac{\pi x_1}{l_2}\right); \ Y_k^{(2)}(x) = \sin\left(\frac{2k-1}{2}\frac{\pi x_2}{l_4}\right) \quad (15)$$

Substituting from Eq. (13) to Eq. (16) and their derivatives into the expression (11) and potential energy expression (12) we have:

$$
\begin{aligned}
T &= \frac{1}{2} I_{O_1} \dot{\varphi}_1^2 + \frac{1}{2} I_{O_2} \dot{\varphi}_3^2 + \frac{1}{2} I_{O_3} \dot{\varphi}_5^2 + \frac{\mu_1 l_1^2 l_2}{2} \dot{\varphi}_1^2 + \frac{\mu_1}{2} \sum_{k=1}^{N_2} \sum_{l=1}^{N_2} b_{kl}^{(1)} \dot{p}_k^{(1)} \dot{p}_l^{(1)} + \frac{\mu_1}{2} \dot{\varphi}_2^2 \sum_{i=1}^{N_1} \sum_{j=1}^{N_1} m_{ij}^{(1)} q_i^{(1)} q_j^{(1)} \\
&+ \frac{\mu_1}{2} \left[\frac{l_2^3}{3} + 2 \sum_{k=1}^{N_2} F_k^{(1)} p_k^{(1)} + \sum_{k=1}^{N_2} \sum_{l=1}^{N_2} b_{kl}^{(1)} p_k^{(1)} p_l^{(1)} \right] \dot{\varphi}_2^2 + \frac{\mu_1}{2} \sum_{i=1}^{N_1} \sum_{j=1}^{N_1} m_{ij}^{(1)} \dot{q}_i^{(1)} \dot{q}_j^{(1)} - \mu_1 l_1 \dot{\varphi}_1 \sin(\varphi_1 - \varphi_2) \sum_{k=1}^{N_2} H_k^{(1)} \dot{p}_k^{(1)} \\
&+ \mu_1 l_1 \dot{\varphi}_1 \dot{\varphi}_2 \cos(\varphi_1 - \varphi_2) \left[\frac{l_2^2}{2} + \sum_{k=1}^{N_2} H_k^{(1)} p_k^{(1)} \right] + \mu_1 l_1 \dot{\varphi}_1 \cos(\varphi_1 - \varphi_2) \sum_{i=1}^{N_1} C_i^{(1)} \dot{q}_i^{(1)} \\
&+ \mu_1 l_1 \dot{\varphi}_1 \dot{\varphi}_2 \sin(\varphi_1 - \varphi_2) \sum_{i=1}^{N_1} C_i^{(1)} q_i^{(1)} - \mu_1 \dot{\varphi}_2 \sum_{i=1}^{N_1} \sum_{k=1}^{N_2} n_{ik}^{(1)} q_i^{(1)} \dot{p}_k^{(1)} + \mu_1 \dot{\varphi}_2 \left[\sum_{i=1}^{N_1} D_i^{(1)} \dot{q}_i^{(1)} + \sum_{i=1}^{N_1} \sum_{k=1}^{N_2} n_{ik}^{(1)} p_k^{(1)} \dot{q}_i^{(1)} \right] \\
&+ \frac{\mu_2 l_3^{*2} l_4}{2} \dot{\varphi}_3^{*2} + \frac{\mu_2}{2} \sum_{k=1}^{N_4} \sum_{l=1}^{N_4} b_{kl}^{(2)} \dot{p}_k^{(2)} \dot{p}_l^{(2)} + \frac{\mu_2}{2} \dot{\varphi}_4^2 \sum_{i=1}^{N_3} \sum_{j=1}^{N_3} m_{ij}^{(2)} q_i^{(2)} q_j^{(2)} \\
&+ \frac{\mu_2}{2} \left[\frac{l_4^3}{3} + 2 \sum_{k=1}^{N_4} F_k^{(2)} p_k^{(2)} + \sum_{k=1}^{N_4} \sum_{l=1}^{N_4} b_{kl}^{(2)} p_k^{(2)} p_l^{(2)} \right] \dot{\varphi}_4^2 + \frac{\mu_2}{2} \sum_{i=1}^{N_3} \sum_{j=1}^{N_3} m_{ij}^{(2)} \dot{q}_i^{(2)} \dot{q}_j^{(2)} - \mu_2 l_3^* \dot{\varphi}_3^* \sin(\dot{\varphi}_3^* - \varphi_4) \sum_{k=1}^{N_4} H_k^{(2)} \dot{p}_k^{(2)} \\
&+ \mu_2 l_3^* \dot{\varphi}_3^* \dot{\varphi}_4 \cos(\dot{\varphi}_3^* - \varphi_4) \left[\frac{l_4^2}{2} + \sum_{k=1}^{N_4} H_k^{(2)} p_k^{(2)} \right] + \mu_2 l_3^* \dot{\varphi}_3^* \cos(\dot{\varphi}_3^* - \varphi_4) \sum_{i=1}^{N_3} C_i^{(2)} \dot{q}_i^{(2)} \\
&+ \mu_2 l_3^* \dot{\varphi}_3^* \dot{\varphi}_4 \sin(\dot{\varphi}_3^* - \varphi_4) \sum_{i=1}^{N_3} C_i^{(2)} q_i^{(2)} - \mu_2 \dot{\varphi}_4 \sum_{i=1}^{N_3} \sum_{k=1}^{N_4} n_{ik}^{(2)} q_i^{(2)} \dot{p}_k^{(2)} + \mu_2 \dot{\varphi}_4 \left[\sum_{i=1}^{N_3} D_i^{(2)} \dot{q}_i^{(2)} + \sum_{i=1}^{N_3} \sum_{k=1}^{N_4} n_{ik}^{(2)} p_k^{(2)} \dot{q}_i^{(2)} \right]
\end{aligned}
\tag{16}
$$

$$
\begin{aligned}
\Pi &= \frac{1}{2} E_1 A_1 \sum_{k=1}^{N_2} \sum_{l=1}^{N_2} p_k^{(1)} p_l^{(1)} g_{kl}^{(1)} + \frac{1}{2} E_1 I_1 \sum_{i=1}^{N_1} \sum_{j=1}^{N_1} q_i^{(1)} q_j^{(1)} k_{ij}^{(1)} \\
&+ \frac{1}{2} E_2 A_2 \sum_{k=1}^{N_4} \sum_{l=1}^{N_4} p_k^{(2)} p_l^{(2)} g_{kl}^{(2)} + \frac{1}{2} E_2 I_2 \sum_{i=1}^{N_3} \sum_{j=1}^{N_3} q_i^{(2)} q_j^{(2)} k_{ij}^{(2)}
\end{aligned}
\tag{17}
$$

where:

$$
C_i^{(1)} = \int_0^{l_2} X_i^{(1)} dx_1 \; ; D_i^{(1)} = \int_0^{l_2} x_1 X_i^{(1)} dx_1 \; ; m_{ij}^{(1)} = \int_0^{l_2} X_i^{(1)} X_j^{(1)} dx_1 \; ; C_i^{(2)} = \int_0^{l_4} X_i^{(2)} dx_2 \quad D_i^{(2)} = \int_0^{l_4} x_2 X_i^{(2)} dx_2 \; ;
$$

$$
m_{ij}^{(2)} = \int_0^{l_4} X_i^{(2)} X_j^{(2)} dx_2 \; ; H_k^{(1)} = \int_0^{l_2} Y_k^{(1)} dx_1 \; ; F_k^{(1)} = \int_0^{l_2} x_1 Y_k^{(1)} dx_1 \; ; b_{kl}^{(1)} = \int_0^{l_2} Y_k^{(1)} Y_l^{(1)} dx_1 \; ; n_{ik}^{(1)} = \int_0^{l_2} X_i^{(1)} Y_k^{(1)} dx_1 \; ;
$$

$$
H_k^{(2)} = \int_0^{l_4} Y_k^{(2)} dx_2 \; ; F_k^{(2)} = \int_0^{l_4} x_2 Y_k^{(2)} dx_2 \; ; \; b_{kl}^{(2)} = \int_0^{l_4} Y_k^{(2)} Y_l^{(2)} dx_2 \; ; \; n_{ik}^{(2)} = \int_0^{l_4} X_i^{(2)} Y_k^{(2)} dx_2 \; ; \; k_{ij}^{(1)} = \int_0^{l_2} X_i^{\prime\prime(1)} X_j^{\prime\prime(1)} dx_1 \; ;
$$

$$
g_{kl}^{(1)} = \int_0^{l_2} Y_k^{\prime(1)} \; Y_l^{\prime(1)} dx_1 \; ; k_{ij}^{(2)} = \int_0^{l_4} X_i^{\prime\prime(2)} X_j^{\prime\prime(2)} dx_2 \; ; \; g_{kl}^{(2)} = \int_0^{l_4} Y_k^{\prime(2)} \; Y_l^{\prime(2)} dx_2
$$

Expressions X_i'' and Y_i' are the derivatives of the corresponding functions with respect to variables x_i, respectively.

Generalized forces: The actuator torque τ of the motor is applied to the input link OA; the friction torques τ_{f_1}, τ_{f_2} and τ_{f_3} are located at the bearings O_1, O_2, O_3 respectively. Ignoring friction at joints B and C. We have:

$$
Q_1 = \tau - \tau_{f_1} \; ; \; Q_3 = -\tau_{f_3} \; ; Q_5 = -\tau_{f_5}
$$

Let s_j be the generalized coordinates consists of the coordinates of the rigid-links φ_1, φ_2, φ_3, φ_4, φ_5 and the modal coordinates of the elastic links q_i, p_k:

$$
\mathbf{s} = \left[\varphi_1 \;\; \varphi_2 \;\; \varphi_3 \;\; \varphi_4 \;\; \varphi_5 \;\; q_1^{(1)} \;\; q_2^{(1)} \;\; \ldots \;\; q_{N_1}^{(1)} \;\; q_1^{(2)} \;\; q_2^{(2)} \;\; \ldots \;\; q_{N_3}^{(2)} \;\; p_1^{(1)} \;\; p_2^{(1)} \;\; \ldots \;\; p_{N_2}^{(1)} \;\; p_1^{(2)} \;\; p_2^{(2)} \;\; \ldots \;\; p_{N_4}^{(2)} \right]^T
$$

Calculate the derivatives for each generalized coordinate s_j in turn, substitute it into (2) to obtain the system of differential equations from (36) to (46), combined with the algebraic equations (6) to (9) to form a system of differential-algebraic equations, represented concisely in the form:

$$
\mathbf{M}(\mathbf{s})\ddot{\mathbf{s}} + \mathbf{\Phi}_s^T(\mathbf{s})\boldsymbol{\lambda} = \mathbf{p}_1(\mathbf{s}, \dot{\mathbf{s}}, t) \tag{18}
$$

$$
\mathbf{f}(\mathbf{s}) = 0 \tag{19}
$$

where: $\mathbf{M}(\mathbf{s})$ is the mass matrix, $\mathbf{f}(\mathbf{s}) = \left[f_1 \;\; f_2 \;\; f_3 \;\; f_4 \right]^T$ is vector of constraint equations, $\boldsymbol{\lambda} = \left[\lambda_1 \;\; \lambda_2 \;\; \lambda_3 \;\; \lambda_4 \right]^T$ is vector of Lagrange multipliers, $\mathbf{\Phi}_s = \partial \mathbf{f} / \partial \mathbf{s}$ is the Jacobi matrix of vector $\mathbf{f}$, $\mathbf{p}_1(\mathbf{s}, \dot{\mathbf{s}}, t)$ is vector the right-hand side of the equations.

The system of equations (18), (19) are general for mechanisms with transverse and longitudinal deformation of flex-links, simpler cases can be derived from the above system of equations. As in the case of the rigid mechanism (all links are rigid), we replace the deformation variables with 0, then we obtain the system of equations written for the rigid mechanism from (47) to (51) (Appendix B) and the connecting equations from (52) to (55) written in the form:

$$\mathbf{M}_R(\mathbf{s}_R)\ddot{\mathbf{s}}_R + \mathbf{\Phi}_{s_R}^T(\mathbf{s}_R)\boldsymbol{\lambda} = \mathbf{p}_{1_R}(\mathbf{s}_R, \dot{\mathbf{s}}_R, t) \tag{20}$$

$$\mathbf{f}_R(\mathbf{s}_R) = 0 \tag{21}$$

where: $\mathbf{s}_R = [\varphi_1 \quad \varphi_2 \quad \varphi_3 \quad \varphi_4 \quad \varphi_5]^T$, $\boldsymbol{\lambda} = [\lambda_1 \quad \lambda_2 \quad \lambda_3 \quad \lambda_4]^T$, $\mathbf{f}_R = [f_{1R} \quad f_{2R} \quad f_{3R} \quad f_{4R}]^T$ and $\mathbf{\Phi}_{s_R} = \dfrac{\partial \mathbf{f}_R}{\partial \mathbf{s}_R}$ are the vectors of the rigid mechanicsm, respectively.

Dynamics analysis

The dynamic model is converted into a general form (18), (19) written for constrained multibody systems, this is a familiar system of equations for a multibody dynamics [1-3]. The system of Eqs. (18) and (19) is very complicated, the analysis of dynamic response can only be solved by numerical methods. There are many ways to solve the above system of equations such as direct solution method, Lagrange multiplier separation method, Lagrange multiplier partition method [29, 30]. These are commonly used methods. The complexity of the calculation and the calculation time depend on the complexity of the model. The model in this study is quite complex, so the numerical calculation is also relatively complex and time-consuming. In this paper, the Lagrange factor partition method is used.

Differentiating Eq. (20) with respect to the time t, we get the equations

$$\dot{\mathbf{f}}(\mathbf{s}) = \frac{\partial \mathbf{f}}{\partial \mathbf{s}}\dot{\mathbf{s}} = \mathbf{\Phi}_s(\mathbf{s})\dot{\mathbf{s}} = \mathbf{0} \tag{22}$$

$$\ddot{\mathbf{f}}(\mathbf{s}) = \mathbf{\Phi}_s(\mathbf{s})\ddot{\mathbf{s}} + \dot{\mathbf{\Phi}}_s(\mathbf{s})\dot{\mathbf{s}} = \mathbf{0} \tag{23}$$

where $\mathbf{\Phi}_s \in \Re^{rxn}$. From (23) we deduce:

$$\mathbf{\Phi}_s\ddot{\mathbf{s}} = -\dot{\mathbf{\Phi}}_s(\mathbf{s})\dot{\mathbf{s}} = \mathbf{p}_2(\mathbf{s}, \dot{\mathbf{s}}) \tag{24}$$

Equations (18) and (24) are rewritten in matrix form as follows:

$$\begin{bmatrix} \mathbf{M} & \mathbf{\Phi}_s^T \\ \mathbf{\Phi}_s & \mathbf{0} \end{bmatrix}\begin{bmatrix} \ddot{\mathbf{s}} \\ \boldsymbol{\lambda} \end{bmatrix} = \begin{bmatrix} \mathbf{p}_1 \\ \mathbf{p}_2 \end{bmatrix} \tag{25}$$

When using numerical methods to solve differential-algebraic equations, due to calculation errors after each integration step, the values $\mathbf{s}(t_k)$, $\dot{\mathbf{s}}(t_k)$ at time t_k no longer satisfy the position and velocity constraint equations:

$$\mathbf{f}(\mathbf{s}_i) \neq \mathbf{0},\ \dot{\mathbf{f}}(\mathbf{s}_i) \neq \mathbf{0}\ (i = 1, 2, ...) \tag{26}$$

According to Baumgarte method [29, 31], instead of solving Eq. (23), we will solve the equation:

$$\ddot{\mathbf{f}} + 2\alpha\dot{\mathbf{f}} + \beta^2\mathbf{f} = \mathbf{0},\ \alpha > 0,\ \beta > 0 \tag{27}$$

The terms $2\alpha\dot{\mathbf{f}}$ **and** $\beta^2\mathbf{f}$ act as control terms. By solving Eq. (27) instead of Eq. (24), we can minimize the accumulated error during the integration process. When we choose α and β as positive constants, we can deduce from the system of Eq. (27):

$$\mathbf{f} \to \mathbf{0} \quad \text{when } t \to \infty.$$

Then the constraint equation $\mathbf{f} = 0$ will be better guaranteed at each calculation step. For constrained multibody systems, this is a key issue when solving the number.

Substituting Eq. (24) into Eq. (27) we get:

$$\mathbf{\Phi}_s\ddot{\mathbf{s}} = -\dot{\mathbf{\Phi}}_s(\mathbf{s})\dot{\mathbf{s}} - 2\alpha\mathbf{\Phi}_s(\mathbf{s})\dot{\mathbf{s}} - \beta^2\mathbf{f}(\mathbf{s}) \tag{28}$$

Put

$$\tilde{\mathbf{p}}_2(\dot{\mathbf{s}}, \mathbf{s}) = -\dot{\mathbf{\Phi}}_s(\mathbf{s})\dot{\mathbf{s}} - 2\alpha\mathbf{\Phi}_s(\mathbf{s})\dot{\mathbf{s}} - \beta^2\mathbf{f}(\mathbf{s}),\ \tilde{\mathbf{p}}_2(\dot{\mathbf{s}}, \mathbf{s}) \in \Re^{rx1}$$

Thus, the system of equations (25) has the form:

$$\begin{aligned} \mathbf{M}(\mathbf{s})\ddot{\mathbf{s}} + \mathbf{\Phi}_s^T(\mathbf{s})\boldsymbol{\lambda} &= \mathbf{p}_1(\mathbf{s}, \dot{\mathbf{s}}, t) \\ \mathbf{\Phi}_s(\mathbf{s})\ddot{\mathbf{s}} &= \tilde{\mathbf{p}}_2(\dot{\mathbf{s}}, \mathbf{s}) \end{aligned} \tag{29}$$

To partition the Lagrange multipliers, we use the orthogonality theorem [29, 30] as

$$\mathbf{\Phi}_s\mathbf{R}=\mathbf{0} \text{ or } \mathbf{R}^T\mathbf{\Phi}_s^T=\mathbf{0} \quad (30)$$

Multiplying both sides of the first equation of (29) by $\mathbf{R}^T$ and using the formula (30) we get:

$$\mathbf{R}^T\mathbf{M}(\mathbf{s})\ddot{\mathbf{s}}=\mathbf{R}^T\mathbf{p}_1(\dot{\mathbf{s}},\mathbf{s},t) \quad (31)$$

$$\mathbf{\Phi}_s(\mathbf{s})\ddot{\mathbf{s}}=\tilde{\mathbf{p}}_2(\dot{\mathbf{s}},\mathbf{s},t) \quad (32)$$

Equations (31) and (32) are ordinary differential equations of generalized coordinates **s**. Numerical solutions to these equations can be done by Newmark, Runge-kutta 4th-order, Runge-Kutta-Nÿstron, etc. methods. However, this is also very time-consuming due to the difficulty of the differential equations.

The analysis of the forward dynamic response and elastic vibration is performed as follows:

+ Using the first three modes in the formulas (12) and (13), i.e. $N_1 = N_2 = N_3 = N_4 = 3$, the coefficients are determined as the formulas from (56) to (69) (Appendix C). We know that the deformations are only concentrated in the first mode, the following modes are very small compared to the first mode, decrease very quickly when the order of modes increases and are insignificant. Most previous studies often use one first mode.

+ To compare the motion of flexible mechanism and the motion of rigid mechanism, this paper performs simultaneous numerical calculations for rigid mechanisms whose dynamic equations have been described by the differential-algebraic equations from (47) to (55).

+ The parameters of mechanism [32]: l_0 =0.3m, l_0^* =0.3m, l_1 = 0.055m, l_2 = 0.259m, l_2 = 0.2m, l_4 = 0.258m, l_5 = 0.22m, $C_1(\xi_{11},\eta_{11})$ = (0.0235, 0) m, $C_2(\xi_{22},\eta_{22})$ = (0.134,0) m, $C_3(\xi_{33},\eta_{33})$ = (0.115, 0.0265) m, $C_4(\xi_{44},\eta_{44})$ = (0.132, 0) m, $C_5(\xi_{55},\eta_{55})$ = (0.113, 0) m, β = 0.3rad, m_1 = 3.02kg, m_2 = 0.165kg, m_3 = 1.84 kg, m_4 = 0.163kg, m_5 = 1.35kg, I_{O1} =51x10^{-4}kgm^2, I_{O2} =183x10^{-4}kgm^2, I_{O3} =115 x10^{-4}kgm^2, E_1 = E_2 = 2.1x10^{11}kgm^{-1}s^{-2}, A_1=81x10^{-6}m^2 and A_2 = 80.5x10^{-6}m^2, I_1 =5.22x10^{-10} m^4 and I_2 =5.15 x10^{-10}m^4, $\theta_1 = \theta_2 = 0$ *rad.*

+ For numerical simulation, the torque acting on the input crank OA is given by:

$$\tau(t)=\begin{cases}\tau_0\sin(2\pi t/T) & t\le T\\ 0 & t\ge T\end{cases} \quad (33)$$

where τ_0 is the amplitude, T is the period of the driving torque. Bearing frictions are neglected.

+ *Initial conditions.* Position and velocity at initial time:

• At the initial moment, the mechanism is stationary at the angular position $\varphi_1(0)$ and angular velocity, we choose:

$$\varphi_1(0)=0,\ \dot{\varphi}_1(0)=0 \quad (34)$$

• The deformation and deformation velocity at the initial time are chosen to be zeros because the mechanism is not moving yet:

$$q_i^{(1)}(0)=q_i^{(2)}(0)=p_i^{(1)}(0)=p_i^{(2)}(0)=0$$
$$\dot{q}_i^{(1)}(0)=\dot{q}_i^{(2)}(0)=\dot{p}_i^{(1)}(0)=0,\dot{p}_i^{(2)}(0)=0 \quad (35)$$

From the Eqs (6) to (9), using the Newton-Raphson method we can solve for the initial values:

$\varphi_2(0)=0.8523(rad)$, $\varphi_3(0)=1.7952(rad)$, $\varphi_4(0)=0.0280(rad)$, $\varphi_5(0)=1.9754(rad)$

Case 1. Numerical calculation results when τ_0 = 3.5Nm, T = 1s

Discussion 1:

+ The figures from Fig. 3a to Fig. 3g are the dynamic response of the mechanism over time when the acting force has the form as in expression , in which the amplitude of the starting torque is chosen $\tau_0 = 3.5$Nm , the period $T = 1$s , besides that the bearing friction is ignored. The analysis time is 3 second . The results show that:

+ The angle of links of the elastic mechanism are solid lines, while the angle of links of the rigid mechanism are dotted lines (from Fig. 3a to Fig. 3c). Thus, the motion of the elastic mechanism has deviations and significant delays compared to the rigid mechanism. In which the deviation of the output links (link 3, link 5) are more obvious than the input link (link 1). This can be explained by the fact that the deformation of flexible link 2 and flexible link 4 directly affects the motion geometry of output links and indirectly affects the input link.

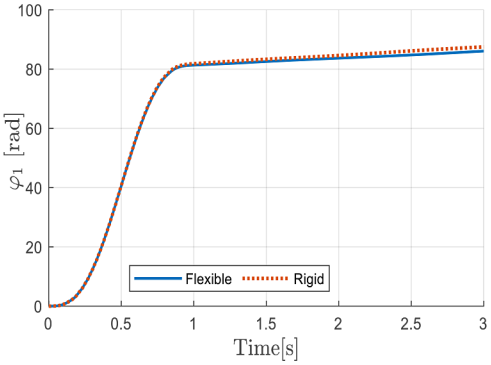

Fig. 3a. Angle of link 1, $\tau_0 = 3.5\text{Nm}$, $T = 1\text{s}$

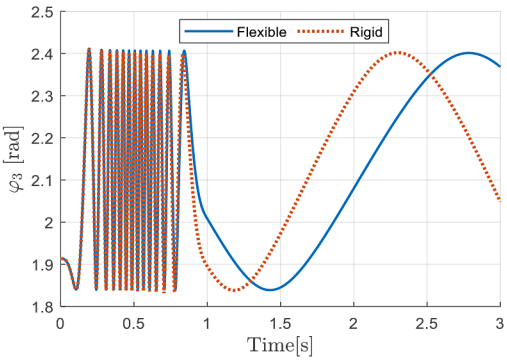

Fig. 3b. Angle of link 3, $\tau_0 = 3.5\text{Nm}$, $T = 1\text{s}$

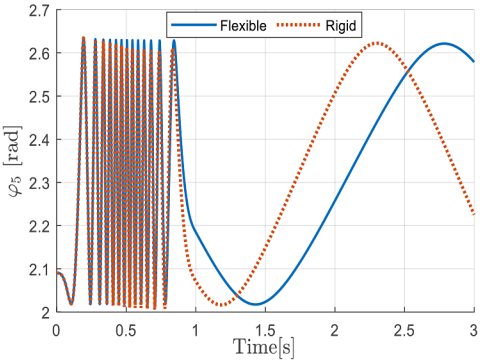

Fig 3c. Angle of link 5, $\tau_0 = 3.5\text{Nm}$, $T = 1\text{s}$

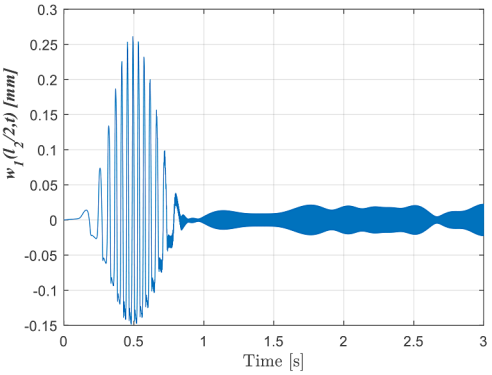

Fig. 3d. Transverse deformation at the middle of the link AB, $\tau_0 = 3.5\text{Nm}$, $T = 1\text{s}$

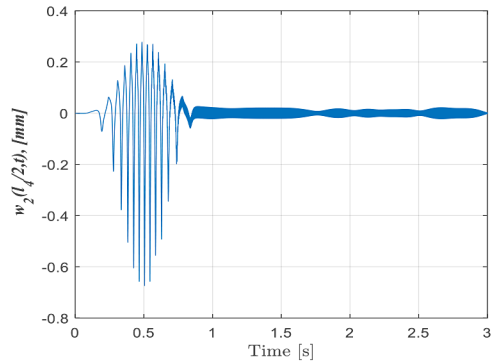

Fig. 3e. Transverse deformation at the middle of the link CD, $\tau_0 = 3.5\text{Nm}$, $T = 1\text{s}$

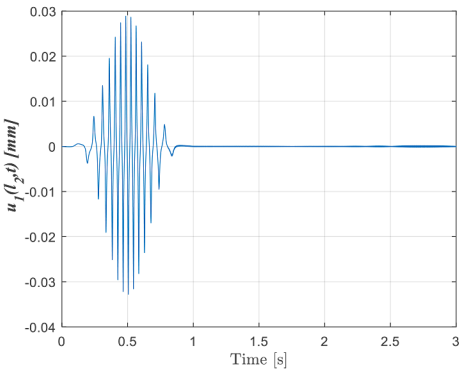

Fig. 3f. Long-deformation at the end of the link AB, $\tau_0 = 3.5\text{Nm}$, $T = 1\text{s}$

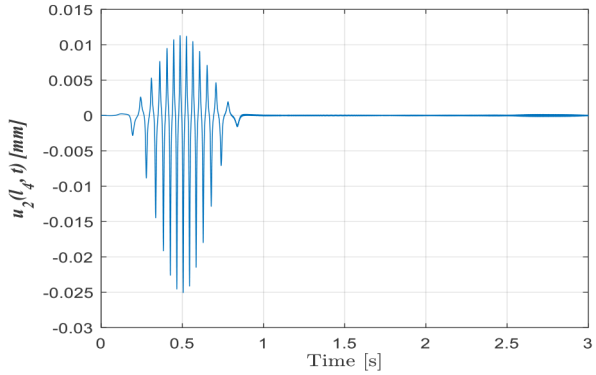

Fig. 3g. Long-deformation at the end of the link CD, $\tau_0 = 3.5\text{Nm}$, $T = 1\text{s}$

+ In Fig. 3d and Fig. 3e are the transverse deformations of flexible connecting rods AB and CD at the middle positions of the rods, and in Fig. 3f and Fig. 3g are their longitudinal deformations at the end points of those bars (point B and D). We see that:

During the time of driving torque ($0 \le t \le T$) these deformation components are significant, they have shapes corresponding to three frequencies of three excitations: the period of the driving torque, the period of movement of the elastic connecting rod and the natural frequency of that connecting rod.

When the torque is no longer applied ($t > T$), the mechanism moves according to inertia, the connecting rods still oscillate elastically, these are free vibrations, the frequency of oscillation depends on the specific properties (stiffness and mass) of the flexible links. These elastic deformations are relatively small compared to the time the torque remains applied.

The amplitude of bending deformation is much larger than the longitudinal deformation, for example, the maximum deformation value of bar CD is about w_{2max} = 0.68 mm, the maximum longitudinal deformation u_{2max} = 0.025 mm. This can be explained by the fact that the bending stiffness (EI) is much smaller than the longitudinal stiffness (EA).

Case 2. Numerical results when increasing the amplitude of the driving torque $\tau_0 = 5\text{Nm}, T = 1\text{s}$

Discusstion 2. The figures from Figure 4a to Figure 4f are the dynamic responses of the mechanism when increasing the amplitude of the driving torque. The results show that:

+ When the amplitude of the driving torque increases, the angle deviation of the links increases (see the excerpt in Figure 4.b), the deformation of the connecting rods increases significantly (see Fig. 4c to Fig. 4f), for example, connecting rod CD has the largest bending deformation w_{2max} = 1.65 mm, the largest longitudinal deformation u_{2max} = 0.055mm. The reason is that when the amplitude of the driving torque increases increases, in addition to the direct force increasing, the speed of the mechanism's movement also increases, leading to increased deformation.

+ When the applied force is no longer applied ($t > T$), the mechanism moves according to inertia, the elastic deformations during this period have increased significantly compared to Case 1. The inertial movement of the mechanism and the vibration of deformations are not damped over time, the reason is that we have ignored the external resistance of the mechanism (bearing friction) and ignored the internal resistance of the connecting rods (internal friction). But even in the case of considering the internal resistance of the connecting rods material, these elastic vibrations will still exist for quite a long time because this resistance is very small.

Case 3. Numerical results when increase the duration of the driving torque $\tau_0 = 5\text{Nm}, T = 1.2\text{s}$

Discusstion 3: When the torque duration increases from T = 1 s to T = 1.2 s (the amplitude remains unchanged), the deformation components increase significantly as shown in Figures 5d to 5g. For example, compared to case 2 when this time period has not been increased, the maximum value of bending deformation w_{2max} of link CD increases from 1.65 mm (Fig. 4d) to 3.8 mm (Fig. 5e), the maximum value of longitudinal deformation u_{2max} increases from 0.055 mm (Fig. 4d) to 0.085 mm (Fig. 5g). When the deformation of the components increases significantly, the position error and delay of the links also increase rapidly as shown in Figures 5a to 5c. The reason is that when increasing the time of force application, the speed of the mechanism also increases. In Figure 5c, we can see that the movement of link 5 shows signs of motion instability.

From the survey of the above cases, it can be seen that it is possible to rely on numerical survey to find the conditions (elastic link size, working speed of the mechanism, etc.) for the deformations of the bars within the allowable limit. As in Case 2, the ratio between the length of the connecting bar CD and its deflection is l_4/w_{2max} = 259/1.65 = 158.5 times, in Case 3 this ratio is l_4/w_{2max} = 259/3.8 = 68.1 times. Thus, in case 2 the deflection is still within the allowable limit (usually in design this ratio can be selected from 150 to 200), but in case 3 the deflection has exceeded the allowable value. In the design of the mechanism, this dynamic deflection cannot be determined without solving this general dynamic problem.

The calculation results for this elastic mechanism are compared with the corresponding rigid mechanism model, which also shows that this elastic model is reliable: when the applied force is small (case 1), the movement of the elastic mechanism deviates little from the rigid mechanism

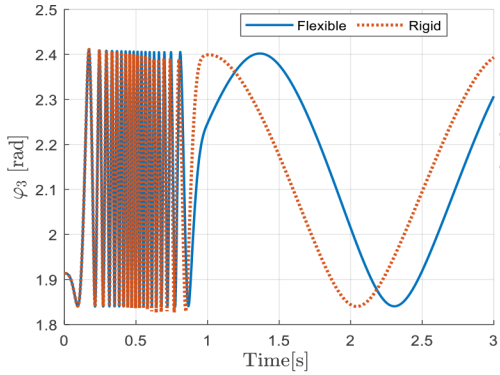

Fig 4a. Angle of link 3, $\tau_0 = 5\text{Nm}, T = 1\text{s}$

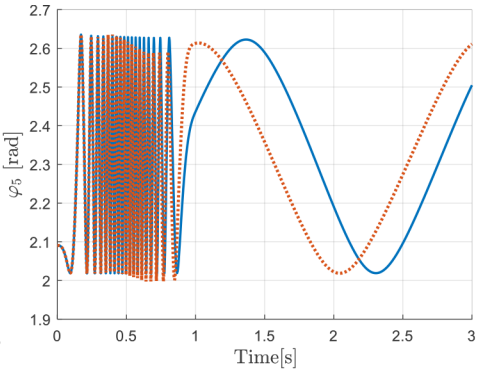

Fig 4b. Angle of link 5, $\tau_0 = 5\text{Nm}, T = 1\text{s}$

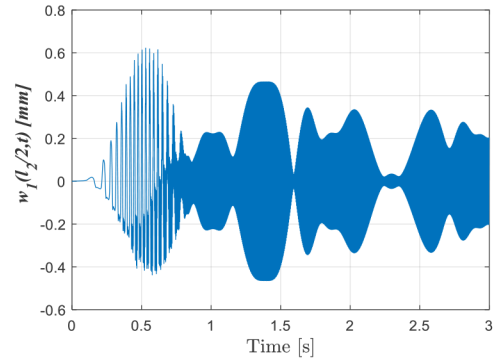

Fig. 4c. Transverse deformation at the middle of the AB-link, $\tau_0 = 5\text{Nm}, T = 1\text{s}$

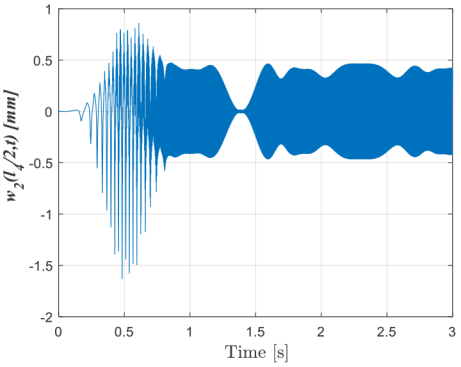

Fig. 4d. Transverse deformation at the middle of the CD-link, $\tau_0 = 5\text{Nm}, T = 1\text{s}$

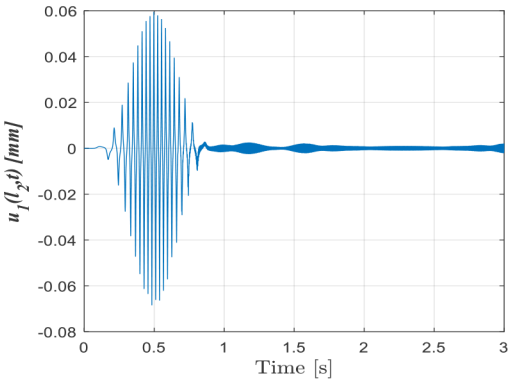

Fig. 4e. Long-deformation at the end of the AB-link, $\tau_0 = 5\text{Nm}, T = 1\text{s}$

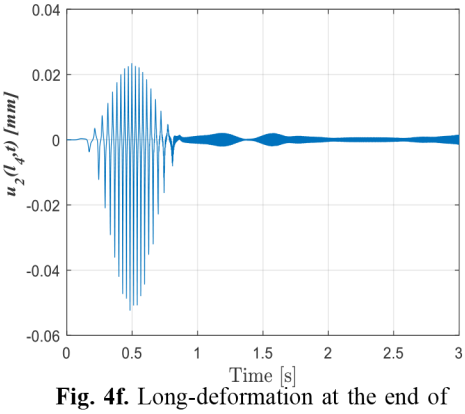

Fig. 4f. Long-deformation at the end of the CD-link, $\tau_0 = 5\text{Nm}, T = 1\text{s}$

and increases when the applied force and force application time increase (Case 2 and 3).

Case 4. Survey with damping. Driving torque parameters $\tau_0 = 5\text{Nm}, T = 1.2\text{s}$. The resistance torques acting on the bearings are selected as:

$$\tau_{f_1} = -\alpha_1\dot{\varphi}_1, \tau_{f_3} = -\alpha_3\dot{\varphi}_3, \tau_{f_5} = -\alpha_5\dot{\varphi}_5$$

$$\alpha_1 = \alpha_3 = \alpha_5 = 0.01\,[\text{Nms}].$$

Note that in this study this friction forces are tentatively chosen for numerical investigation.

Discussion 4: In the Figures 6a to 6d, the dynamic responses of the mechanism when there is friction resistance at the bearings. In Fig. 6a, we see that bearing friction affects the movement of the input link the most. Fig. 6c and Fig. 6d of the link CD are reduced compared to those without friction (in Case 3). The signs of motion instability as mentioned in Case 3 are also gone, the free deformations are still maintained but reduced. Thus, these resistance components contribute to reducing the influence of deformation on the movement of the output link.

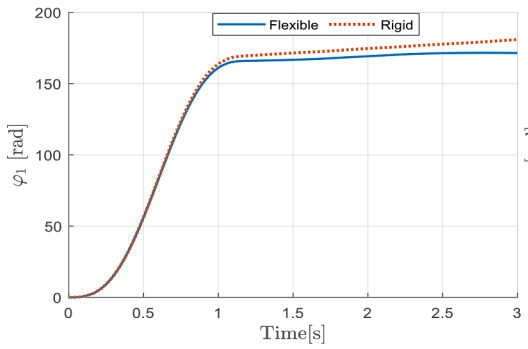

Fig. 5a. Angle of link 1, $\tau_0 = 5\text{Nm}$, $T = 1.2\text{s}$

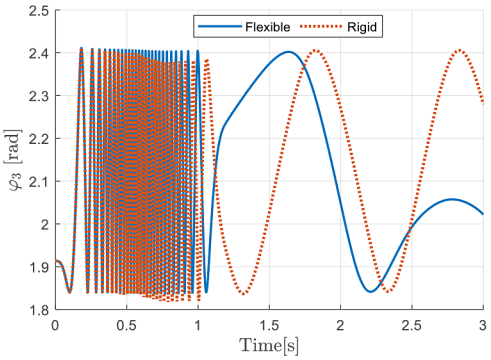

Fig. 5b. Angle of link 3, $\tau_0 = 5\text{Nm}$, $T = 1.2\text{s}$

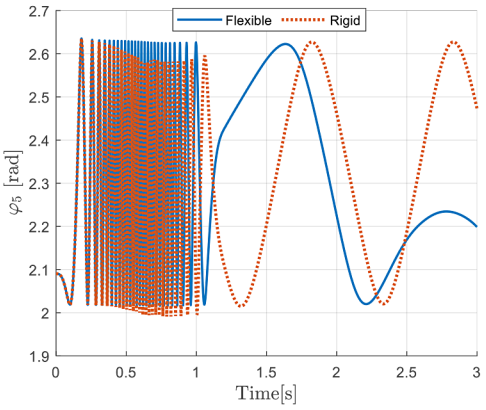

Fig. 5c. Angle of link 5, $\tau_0 = 5\text{Nm}$, $T = 1.2\text{s}$

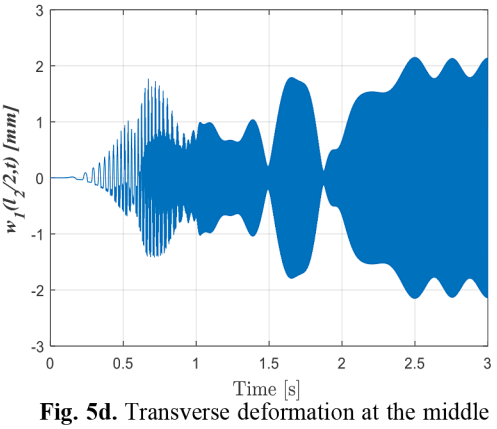

Fig. 5d. Transverse deformation at the middle of the AB-link, $\tau_0 = 5Nm$, $T = 1.2s$

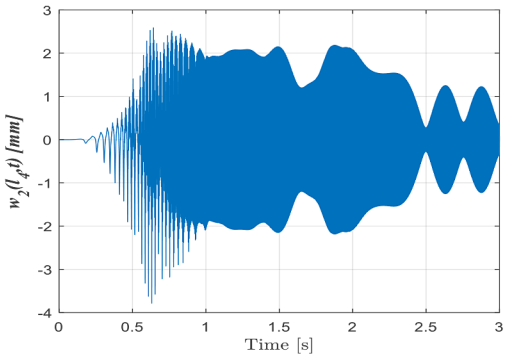

Fig. 5e. Transverse deformation at the middle of the CD-link, $\tau_0 = 5Nm$, $T = 1.2s$

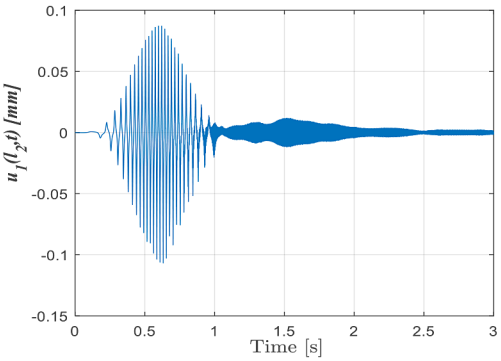

Fig. 5f. Long-deformation at the end of the AB-link, $\tau_0 = 5Nm$, $T = 1.2s$

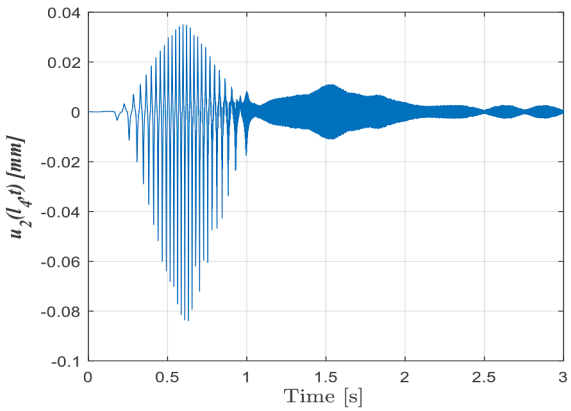

Fig. 5g. Long-deformation at the end of the CD-link, $\tau_0 = 5Nm$, $T = 1.2s$

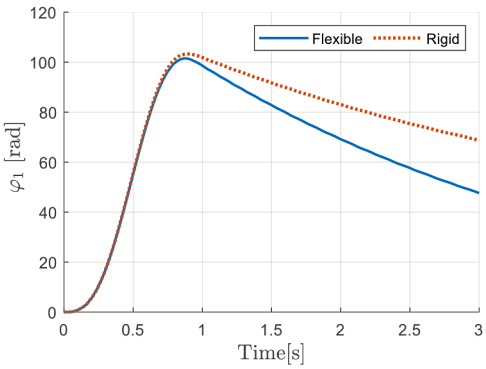

Fig. 6a. Angle link 1, $\tau_0 = 5\text{Nm}$, $T = 1.2\text{s}$ with bearing friction

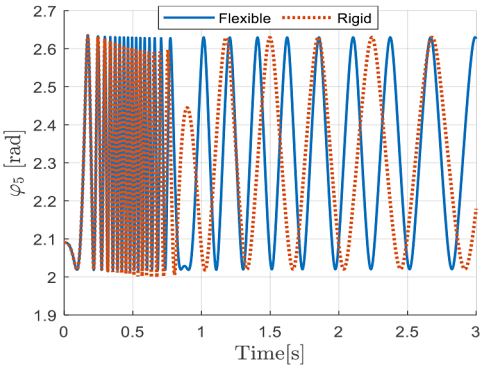

Fig. 6b. Angle link 3, $\tau_0 = 5\text{Nm}$, $T = 1.2\text{s}$ with bearing friction

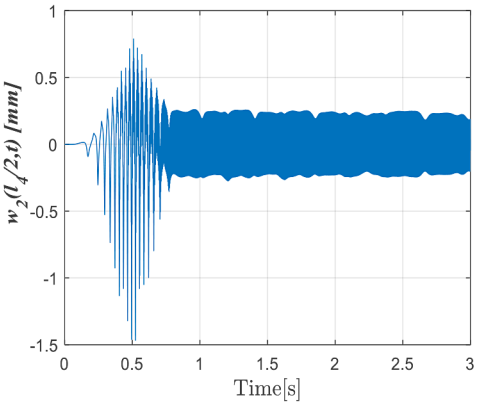

Fig. 6c. Transverse deformation at the middle of the CD link, $\tau_0 = 5Nm, T = 1.2s$, with bearing friction

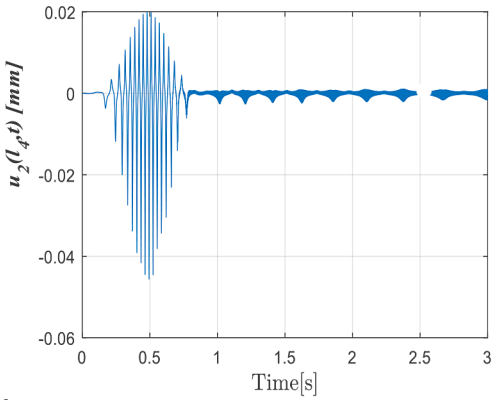

Fig. 6d. Long-deformation at the end of the CD-link, $\tau_0 = 5Nm, T = 1.2s$, with bearing friction

CONCLUSIONS

With the aim of investigating the influence of elastic deformation on motion, working accuracy, and motion delay, this study developed a dynamic model for a flexible six-bar linkage mechanism based on a selected mechanical model formed by coupling two four-bar linkage mechanisms. This model was then used to analyze the motion of the flexible mechanism and compare it with that of a rigid mechanism. The results draw some comments as follows:

1. The dynamic model of the elastic mechanism is built as a general model and reliable model, with elastic connecting rods, the system of equations describing the motion is a system of nonlinear differential-algebraic equations. Simpler cases such as rigid mechanisms, elastic mechanisms with connecting rods considering only bending deformation, elastic mechanisms with connecting rods considering only longitudinal deformation can all be derived from the above general system of equations.
2. From this system of dynamic equations, we can use it to: investigate the dynamic response of the mechanical system; investigate the periodic oscillation of the elastic mechanism; linearize and investigate the stability of the motion; or control the motion and elastic oscillation of the mechanism to move as desired.
3. Numerical simulation results for several cases indicate that the motion of the flexible mechanism exhibits significant deviation and delay compared to the rigid mechanism. Among these, the deviations of the output links (3, 5) are more pronounced than those of the input link (1). During the force application period ($0 \le t \le T$), the deformation components are considerable, corresponding to three frequencies: the excitation frequency of the driving torque, the motion frequency of the connecting rod, and the natural frequency of the connecting rod. After the force application ends ($t > T$), the connecting rods continue to exhibit elastic oscillations, and the elastic deformations remain significant during this period, especially when

the driving torque or force application duration increases. This is because such increases lead to higher mechanism motion speeds. Analyzing the elastic oscillations of the flexible connecting rods can provide insights for designing mechanisms in terms of strength, deflection, and other parameters, or determining the maximum allowable operating speed for the mechanism.

4. This study is limited to numerical investigations of the forward dynamics of the mechanism. Research on inverse dynamics, motion control, and vibration control can also be conducted based on the developed dynamic model. These topics are highly interesting but relatively complex due to the challenges posed by the extended coordinates of the flexible mechanism, which include elastic deformations that are difficult or impossible to control directly. As such, controlling flexible mechanisms can be classified as underactuated control.

REFERENCES

1. Shabana A.A. (1997), Flexible multibody dynamics: Review of past and recent developments, Multibody System Dynamics 1, 189-222. https://doi.org/10.1023/A:1009773505418.
2. Bauchau, O.A. (2011). Flexible multibody systems: preliminaries. In: Flexible Multibody Dynamics. Solid Mechanics and Its Applications, 176. Springer, Dordrecht. https://doi.org/10.1007/978-94-007-0335-3_15
3. Bremer H. (2008), Elastic Multibody Dynamics. A Direct Ritz Approach, Springer, Berlin.
4. M. Geradin, A. Cardona (2001), Flexible Multibody Dynamics/ A Finite Element Approach. John Wiley&Sohns, Chicester.
5. Simeon B. (2013), Computational Flexible Multibody Dynamics, Springer, Berlin.
6. Dwivedy S.K., Eberhard P. (2006), Dynamic analysis of flexible manipulators, a literature review, Mechanism and Machine Theory 41, 749–777. https://doi.org/10.1016/j.mechmachtheory.2006.01.014.
7. Ankarali A., Diken H. (1997), Vibration control of an elastic manipulator link, Journal of Sound and Vibration 204, 162–170. https://doi.org/10.1006/jsvi.1996.0897
8. Hill, D. E. (2012), Dynamics and control of a rigid and flexible four bar coupler. Journal of Vibration and Control 20(1), 131-145. https://doi.org/10.1177/1077546312462917.
9. Karkoub, M. and Yigit. A.S. (1999), Vibration control of a four-bar mechanism with a flexible coupler, Journal of Sound and Vibration 222(2), 171-189. https://doi.org/10.1006/jsvi.1998.2080
10. Van Khang, N., Nam, N.S., Dien, N.P. (2019). Modelling and Model-Based Control of a Four-Bar Mechanism with a Flexible Coupler Link. In: (Chunhui) Yang, R., Takeda, Y., Zhang, C., Fang, G. (eds) Robotics and Mechatronics. ISRM 2017. Mechanisms and Machine Science, 72. Springer, Cham. https://doi.org/10.1007/978-3-030-17677-8_6.
11. Masurekar V., Gupta K.N. (1988), Stability analysis of four bar mechanism. Part I With the assumption that damping is absent, Mechanism and Machine Theory 23(5), 367-375. https://doi.org/10.1016/0094-114X(88)90051-1.
12. Yang K.H., Park Y.S. (1998), Dynamic stability analysis of a flexible four-bar mechanism and its experimental investigation, Mechanism and Machine Theory 33(3), April 1998, 307–320. https://doi.org/10.1016/S0094-114X(97)00048-7
13. Gatti G., Mundo D. (2010), On the direct control of follower vibrations in cam–follower mechanisms, Mechanism and Machine Theory 45(1), 23-35. https://doi.org/10.1016/j.mechmachtheory.2009.07.010
14. Zhang C. and Yan H.S. (2000), Motion control of cam mechanisms, Mechanism and Machine Theory 35(4), April 2000, 593–607. https://doi.org/10.1016/S0094-114X(99)00025-7
15. Beale D.G. and Lee S.W. (1995), The applicability of fuzzy control for flexible mechanisms, ASME Design Engineering Technical Conferences DE 84(1), 203-209.
16. Liao W. H., Chou J. H. and Horng I. R. (1997), Robust vibration control of flexible linkage mechanisms using piezoelectric films, Smart Materials and Structures 6, 457-463. https://doi.org/10.1088/0964-1726/6/4/010
17. Pashechko, M., Pasika, V., Hembara, N., Kharzhevskyi, V. (2020). Analysis of Linkage Mechanisms with Internal Driving Link. Advances in Science and Technology Research Journal, 14(1), 191-200. https://doi.org/10.12913/22998624/117426
18. Sung C.K. and Chen Y.C. (1991), Vibration Control of the Elastodynamic Response of High-Speed Flexible Linkage Mechanisms, Journal of Vibration and Acoustics 113(1), 14-21. https://doi.org/10.1115/1.2930148
19. Gonzalez F., Masarati P., Cadrado J., Naya M.A. (2017), Asessment of linearization approaches for multibody dynamics formulations. ASME Journal of Computational and Nonlinear Dynamics 12, 041009-1 - 041009-7. https://doi.org/10.1115/1.4035410
20. Khalil W., Gautier M. (2000). Modeling of mechanical systems with lumped elasticity. Proceedings of the IEEE International Conference on Robotics and Automation 4, 3964–3969. https://doi.org/10.1109/ROBOT.2000.845349.

21. Negrut D., Ortiz J.L. (2006). A Practical Approach for the Linearization of the Constrained Multibody Dynamics Equations. ASME Journal of Computational and Nonlinear Dynamics.
22. Peterson D. L., Gede G., Hubbard M. (2015). Symbolic linearization of equations of motion of constrained multibody systems. Multibody Syst Dyn 33, 143-161.
23. Van Khang, N., Sy Nam, N. & Van Quyen, N (2018). Symbolic linearization and vibration analysis of constrained multibody systems. Arch Appl Mech 88, 1369–1384. https://doi.org/10.1007/s00419-018-1376-8
24. Gordon R. Pennocka, Ali Israrb (2009), Kinematic analysis and synthesis of an adjustable six-bar linkage, Mechanism and Machine Theory, 44, 306–323. https://doi.org/10.1016/j.mechmachtheory.2008.04.007.
25. Zhan Wei, Zanyong Wang, Dandan Li and Dong Liang (2024). Rigid-flexible coupling dynamic modelling and dynamic accuracy analysis of planar cam four-bar mechanism with multiple clearance joints. Proceedings of the Institution of Mechanical Engineers, Part K: Journal of Multibody Dynamics, 238(3), 421–444. https://doi.org/10.1177/14644193241264076
26. Zhang, Z., Wang, L., Liao, J., Zhao, J., Yang, Q. (2021). Rigid-flexible coupling dynamic modeling and performance analysis of a bioinspired jumping robot with a six-bar leg mechanism. Journal of Mechanical Science and Technology 35(8). https://doi.org/10.1007/s12206-021-0737-3
27. Chen, X., Jiang, S. & Wang, T. (2022). Dynamic modeling and analysis of multi-link mechanism considering lubrication clearance and flexible components. Nonlinear Dyn 107, 3365–3383. https://doi.org/10.1007/s11071-021-07130-7
28. Kharzhevskyi, V. O. (2017). Kinematic synthesis of linkage mechanisms using burmester points at the given dwell duration of the output link. Advances in Science and Technology Research Journal, 11(2), 139-145. https://doi.org/10.12913/22998624/68465
29. Shabana, A. A. (2020). Dynamics of Multibody Systems. Cambridge: Cambridge University Press.
30. DeJalon, J.G., Bayo, E. (1994), Kinematic and Dynamic Simulation of Multibody Systems. Springer, New York.
31. Baumgarte, J. (1972), Stabilization of constraints and integrals of motion in dynamic systems. Comput. Methods Appl. Mech. Eng. 1, 1–16. https://doi.org/10.1016/0045-7825(72)90018-7
32. Khang, N., V. (1986), Dynamische Stabilität und periodische Schwingungen in Mechanismen. Diss. B, TH Karl-Marx-Stadt.
33. Cepolina E. E., Zaplana I., D'Imperio M. P., Gagliardi R., Baizid K., Scaccia M., Dai J., Muscolo G., Cannella F. (2021), Scalable six bar linkage mechanism for re-orienting and aligning objects: Design methodology, Procedia CIRP, 97, 66-70, https://doi.org/10.1016/j.procir.2020.05.205.
34. Plecnik, M. M. (2015). The Kinematic Design of Six-bar Linkages Using Polynomial Homotopy Continuation. UC Irvine. ProQuest ID: Plecnik_uci_0030D_13436. Merritt ID: ark:/13030/m5rr45f6. Retrieved from https://escholarship.org/uc/item/3sb8s541.